Metallophysics and Advanced Technologies
Металофіз. новітні технол.
Metallofiz. Noveishie Tekhnol.
2024, vol. 46, No. 9, pp. 893–914
https://doi.org/10.15407/mfint.46.09.0893
Reprints available directly from the publisher

PACS numbers: 06.60.Vz, 42.62.Cf, 61.72.Ff, 81.05.Bx, 81.20.Vj, 81.30.Kf, 81.70.Bt

Specifics of Creating Joints from Modern Boron-Microalloyed High-Strength Steels Utilizing Laser, Contact Spot, as Well as Argon-Arc Spot Welding Technologies

G. Polishko, Yu. Kostetskyi, V. Kostin, Ye. Pedchenko,
A. Bernatskyi, M. Sokolovskyi, P. Honcharov, and V. Zaitsev

E. O. Paton Electric Welding Institute, N.A.S. of Ukraine,
11 Kazymyr Malevych Str.,
UA-03150 Kyiv, Ukraine

In this study, an analysis of current welding technologies for new high-strength low-alloyed AHSS sheet steels is presented. Over the course of it, a series of welded joints of sheet metal with a thickness of 1.2 mm made of CR1000Y1370T-CH steel (composition: 0.23% C, 2% Si, 3% Mn, 0.015–2% Al, 1% Cr + Mo, 0.15% Ti + Nb, 0.2% Cu) by Voelstalpine (Austria) is investigated. The joints are produced using laser, spot, and argon-arc spot welding under specified conditions. High-quality weld joints are obtained through laser welding with the formation of a dispersed ferrite–bainite structure with an acceptable hardness level (up to 4000 MPa) without martensitic-type structures and zinc evaporation from the sheet coating along the entire length of the welded joint. As discovered, due to delamination and remnants of zinc coating, it is not possible to achieve a high quality of weld joints while using spot welding, as well as argon-arc spot welding. The selected welding conditions for these technologies are found to be ineffective and require further refinement.

Key words: AHSS steel, laser welding, argon-arc spot welding, spot welding, microstructure, ferrite, bainite, martensite.

У роботі представлено аналізу сучасних технологій зварювання нових високоміцних низьколеґованих листових криць AHSS. Досліджено серію

Corresponding author: Ganna Oleksiyivna Polishko
E-mail: ganna.polishko@gmail.com

Citation: G. Polishko, Yu. Kostetskyi, V. Kostin, Ye. Pedchenko, A. Bernatskyi, M. Sokolovskyi, P. Honcharov, and V. Zaitsev, Specifics of Creating Joints from Modern Boron-Microalloyed High-Strength Steels Utilizing Laser, Contact Spot, as Well as Argon-Arc Spot Welding Technologies, *Metallofiz. Noveishie Tekhnol.*, **46**, No. 9: 893–914 (2024). DOI: 10.15407/mfint.46.09.0893

зварних з'єднань листового металу товщиною у 1,2 мм з криці CR1000Y1370T-CH (склад: 0,23% C, 2% Si, 3% Mn, 0,015–2% Al, 1% Cr + Mo, 0,15% Ti + Nb, 0,2% Cu) виробництва компанії Voelstalpine (Австрія). З'єднання виконували лазерним, точковим та арґонодуговим точковим зварюванням за визначених умов. Якісні зварні з'єднання було одержано лазерним зварюванням з утворенням дисперсної феритно-бейнітної структури з прийнятним рівнем твердости (до 4000 МПа) без структур мартенситного типу та випаровування Цинку з покриття листа уздовж всієї довжини зварного з'єднання. Було виявлено, що через відшарування та залишки цинкового покриття неможливо досягти високої якости зварних з'єднань з використанням точкового зварювання й арґонодугового точкового зварювання. Вибрані режими зварювання за цими технологіями виявилися неефективними та потребують подальшого доопрацювання.

Ключові слова: криця AHSS, лазерне зварювання, арґонодугове точкове зварювання, точкове зварювання, мікроструктура, ферит, бейніт, мартенсит.

(Received 9 January, 2024; in final version, 11 April, 2024)

1. INTRODUCTION

Recently, the practice of using advanced high strength steel (AHSS) for the manufacture of car bodies has spread throughout the car manufacturing industry [1–5]. The use of steels of this type allows reducing the thickness of the rolled sheet used for the manufacture of body parts, while maintaining the strength of the structure. At the same time, its weight and the car as a whole are reduced, which contributes to the reduction of harmful emissions into the environment during its operation [3, 4].

AHSS steels differ from traditional structural steels in both chemical composition and microstructure [6–8]. They are characterized by a unique combination of strength and plasticity, which is achieved by the specifically selected chemical composition as well as its multiphase microstructure, which forms as a result of carefully controlled deformation and heat treatment [3–5, 9]. Intensive heat input during welding and subsequent cooling, generally causes significant changes in the microstructure of the metal in the heat affected zone (HAZ), due to recrystallization, increasing grain sizes and separation of phases at their boundaries. An example of such processes would be the well-known formation of martensitic and/or bainite microstructure in metal under conditions of rapid cooling, characteristic of most welding processes [8, 10]. However, changes in the AHSS's microstructure that occurs in the HAZ during welding can be critical and lead to the loss of specified properties, as they are achieved primarily due to the controlled microstructure. Therefore, the choice of modes and methods of joining these

steels is associated with certain problems and requires careful control of the process parameters [7, 10, 11].

Today, many various welding processes, which can be used in the automotive industry to join parts out of AHSS steels, exist [3, 4, 11]. Each of them has certain features that determine the expediency of its usage in various specific conditions [3, 9–11]. In addition to welding processes, adhesive (gluing) and mechanical connection technologies, various soldering methods, as well as hybrid connection processes can be used to connect parts from AHSS steels [3, 4, 12–15].

However, welding remains the main method of connecting metal automotive body parts. In particular, electric arc welding, which belongs to a family of processes based on strong heating by an electric arc of the edges of the connecting parts of the parts until they melt for welding, is wildly used in car manufacturing [3, 4, 10]. At the same time, *via* using this method, additional additive material can also be introduced into the melting zone [11]. Arc welding is sometimes referred to as one of the 'low-tech' processes; however, its popularity is steadily high, primarily due to the low-cost equipment and high application flexibility [10]. However, joining products made from AHSS steels by electric arc welding is associated with significant problems and limitations, mainly due to the difficulty of preventing the oxidizing effect of atmospheric air and localizing the thermal effect on the welded material.

Contact welding is widely used to connect steel body parts in modern automobile manufacturing, when the connection is formed as a result of the introduction of two types of energy—thermal, that appears from the passage of an electric current, and mechanical, that appears due to the application of external force. There are many options for implementing such a process, but the most commonly used one is resistance spot welding (RSW) [3, 10]. As it is known, RSW is characterized by an intensive mechanical compression of the connecting surfaces in the joint area with the possibility of changing the clamping force during the flow of welding current and forging, intensive mixing of the molten metal, short heating and cooling time, the possibility of pre- and re-heating during welding cycle, absence of the heated metal oxidation, possible adjustment of the heating and cooling speed, full process automation, *etc*. In addition, resistance seam welding (RSW) and resistance projection welding (RPW) are also widely used in the automotive industry [10, 11].

The body design of some automobiles, as well as some complex parts, excludes the possibility of spot welding usage. In such cases, gas metal arc welding (GMAW) or tungsten inert gas (TIG) welding are usually used [12, 16]. These and similar arc welding methods are used to join products from AHSS steels in the same way they are used for low carbon steels. At the same time, during the welding of AHSS steels, same shielding gases can be used as when welding low-carbon steels [3, 4,

11]. On the other hand, welding of AHSS steels requires control that is more careful and maintenance of specified process parameters.

The lowest overall thermal load on the workpiece during welding is provided by the processes, which involve focusing the energy, required for the joint formation on very small areas [10]. This achieves a minimal change in the base metal properties as well as minimal residual stresses and deformations [3], allowing the welding process to be carried out at sufficiently high speeds [11]. The main options for implementation of such processes with exceptional point density of energy are laser beam welding (LBW) [17–19] and electron beam welding (EBW) [4, 10, 20, 21]. Since EBW requires vacuum conditions for proper functioning, laser welding has become the most common in the automotive industry.

Compared to traditional arc welding processes, laser welding provides significantly smaller HAZ dimensions, which is important for AHSS steel joints [20]. The ability to focus the laser beam allows for a significant reduction of the weld area width and, accordingly, the HAZ [21]. The most common types of installations used in the industry for processing materials with laser radiation, and in particular, welding, are CO_2, solid-state (Nd:YAG), fibre and diode lasers [3, 22–25].

Thus, the modern industry, in particular the automobile industry [3, 5, 7, 10], in the railway industry [26–31] and other industries [32–34], has a fairly wide selection of welding connection technologies, which allows choosing the most rational options for welding structural elements in accordance with specific conditions and properties of materials that combine.

The purpose of this study is to determine the influence of methods of part welding (laser, contact-spot, argon-arc spot) from thin sheet steels, common for the automotive industry, on the nature of changes in the microstructure of a sheet of metal from modern high-strength steel, microalloyed with boron, with a zinc coating, and to determine the most promising method and the welding mode, which ensures the creation of a high quality welded joint.

2. EXPERIMENTAL/THEORETICAL DETAILS

In this work, the test samples of welded joints were obtained under different welding modes by methods commonly used in the production of sheet steel parts in the automotive industry—contact spot welding, argon-arc spot welding on the tip, and laser welding. The applied welding modes were recommended by specialists of the relevant departments of E. O. Paton Electric Welding Institute, N.A.S. of Ukraine, for welding of 1.2 mm thick sheets of CR1000Y1370T-CH-EG53/53-U steel (Table 1), manufactured by Voelstalpine (Austria), a typical SP AHSS steel.

TABLE 1. Chemical composition of CR1000Y1370T-CH steel (% mass.).

C, max	Si, max	Mn, max	P, max	S, max	Al	Cr + Mo, max	Ti–Nb, max	B, max	Cu, max
0.23	2.0	3.0	0.050	0.010	0.015–2.0	1.0	0.15	0.005	0.2

Modern methods of physical materials science were used to assess the influence of various technologies and welding modes on the properties and structure of the metal of welded joints, such as: optical microscopy of micro- and macrostructure ('NEOPHOT-32' microscope), SEM using JSM-840 'JEOL', energy dispersive microanalysis (EDS) using INCA Energy 450 'Oxford Instruments' system (resolving power is 1 nm, detector sensitivity is 133 eV/10 mm^2), hardness determination methods *via* durometric analysis utilizing a M-400 'LECO' hardness tester.

2.1. Contact Spot Welding Technique

A contact welding machine TECNA 4647 (Italy) was used to obtain a contact spot welding joint. Over the course of the experiments, a number of technological working modes with different parameters of the welding process—clamping force, welding current, duration of clamping, duration of welding, *etc.* were tested. A total of 11 welding modes were tested (provided in Table 2). The general appearance of the welding cyclogram is shown on Fig. 1.

Preliminary analysis/calculation determined, that for a sheet with a thickness of 1.2 + 1.2 mm, which was subjected to welding, it is necessary to obtain the diameter of the welding point of $\varnothing t = 5.0–6.0$ mm. The electrodes of the contact-welding machine are formed by a hemisphere for the analysis of welding modes during the formation of a point connection. The appearance of the resulting welded joints, as well as the welding process is shown in Fig. 2.

2.2. Argon-Arc Spot Welding Technique

A EWM Tetrix 230 AC/DC welding current source with a non-fusible electrode was used for argon-arc spot welding. The appearance of welded joints and the welding process is shown in Fig. 3.

During welding, the parts to be joined were pressed by the specialized nozzle using manual force, with the subsequent enabling of the welding machine for a set period of time. With such pressure, the force usually does not exceed 50 kgf (up to 500 N) and is small compared to the pressure force that occurs during contact spot welding.

TABLE 2. Contact spot welding modes and results.

Sample	Welding mode	Results
1	2	3
1	Pressing force $P_w = 2.5$ kN, welding current $I_w = 2.5$ kA, duration of pressing parts $t_{pr} = 0.1$ s, welding duration $t_w = 0.2$ s, forging duration $t_{for} = 0.1$ s	Insufficient spot weld diameter
2	Pressing force $P_w = 3$ kN, welding current $I_w = 2.8$ kA, duration of pressing parts $t_{pr} = 0.1$ s, welding duration $t_w = 0.2$ s, forging duration $t_{for} = 0.1$ s	Insufficient spot weld diameter
3	Pressing force $P_w = 3$ kN, welding current $I_w = 3$ kA, duration of pressing parts $t_{pr} = 0.1$ s, welding duration $t_w = 0.25$ s, forging duration $t_{for} = 0.1$ s	Spot weld formed
4	Pressing force $P_w = 3.2$ kN, welding current $I_w = 3$ kA, duration of pressing parts $t_{pr} = 0.1$ s, welding duration $t_w = 0.25$ s, forging duration $t_{for} = 0.1$ s	Spot weld formed
5	Pressing force $P_w = 3.4$ kN, welding current, $I_w = 3$ kA, duration of pressing parts $t_{pr} = 0.1$ s, welding duration $t_w = 0.3$ s, forging duration $t_{for} = 0.1$ s	Spot weld formed
6	Pressing force $P_w = 3.5$ kN, welding current $I_w = 3.1$ kA, duration of pressing parts $t_{pr} = 0.1$ s, welding duration $t_w = 0.32$ s, forging duration $t_{for} = 0.1$ s	Spot weld formed
7	Pressing force $P_w = 3.5$ kN, welding current $I_w = 3.2$ kA, duration of pressing parts $t_{pr} = 0.1$ s, welding duration $t_w = 0.35$ s, forging duration $t_{for} = 0.1$ s	Spot weld formed
8	Pressing force $P_w = 3.5$ kN, welding current $I_w = 3.2$ kA, duration of pressing parts $t_{pr} = 0.1$ s, welding duration $t_w = 0.35$ s, forging duration $t_{for} = 0.1$ s	Spot weld formed
9	Pressing force $P_w = 3.5$ kN, welding current $I_w = 3.5$ kA, duration of pressing parts $t_{pr} = 0.1$ s, welding duration $t_w = 0.32$ s, forging duration $t_{for} = 0.1$ s	Spot weld formed
10	Pressing force $P_w = 3.5$ kN, welding current $I_w = 3.5$ kA, duration of pressing parts $t_{pr} = 0.1$ s, welding duration $t_w = 0.35$ s, forging duration $t_{for} = 0.1$ s	Spot weld formed
11	Pressing force $P_w = 3.5$ kN, welding current $I_w = 3.5$ kA, duration of pressing parts $t_{pr} = 0.1$ s, welding duration $t_w = 0.4$ s, forging duration $t_{for} = 0.1$ s	Diameter of the spot weld core increased to 7.4 mm, pointing to an excessive welding mode

During the experiments, 9 welding modes were tested, which differed in such welding process parameters—welding time, current rise

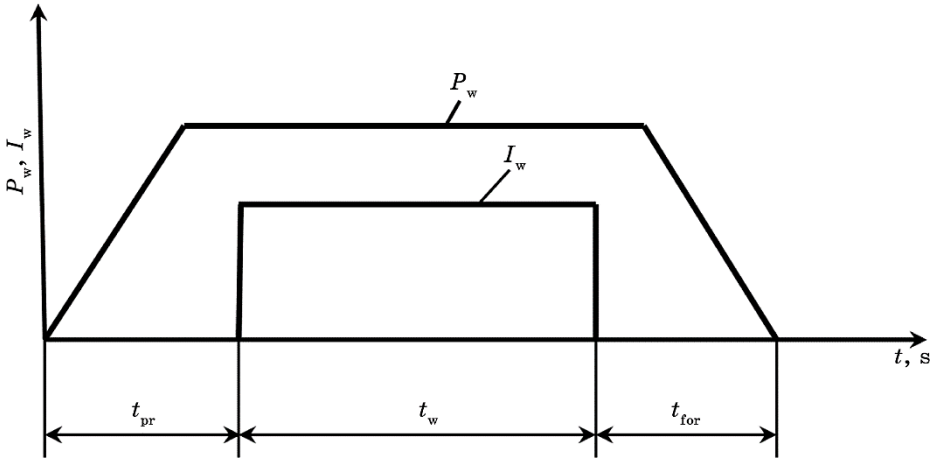

Fig. 1. Welding cyclogram for contact spot welding: P_w is pressing force, daN, I_w is welding current, kA, t_{pr} is the duration of pressing parts, t_w is duration of welding, t_{for} is duration of forging.

a *b*

Fig. 2. The appearance of the welded joints (*a*) and the process of contact spot welding (*b*).

time, current fall time, welding current, arc voltage (Table 3).

The diameter of the tungsten electrode, its sharpening angle, and the argon consumption rate were the same for all test-welding modes

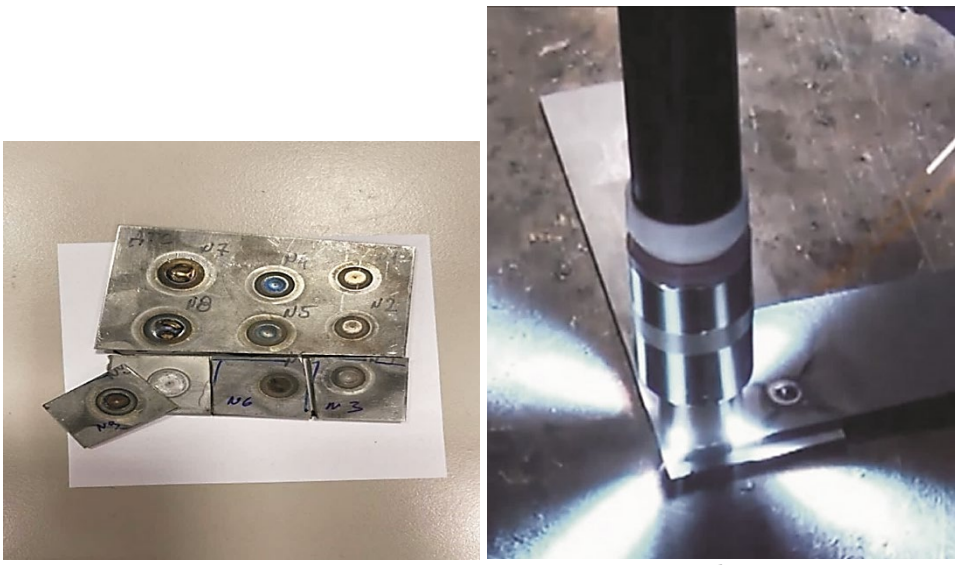

a *b*

Fig. 3. Appearance of welded joints (*a*) and the process of argon-arc spot welding (*b*).

and were 2.4 mm, 30°, and 12 l/min, respectively. The general appearance of the welding cyclogram is shown in Fig. 4.

2.3. Laser-Welding Methodology

Welded joints were performed taking the direction of deformation (along and across the rolling direction) into the account using a solid-state Nd:YAG 'DY-044' laser. For this process, a welding head with a lens with a focal length of 300 mm was used. Welding modes are listed in Table 4. The amount of defocusing of laser radiation for all experiments is $\Delta F = -0.7$ mm. A gas protection system with 20 l/min CO_2 consumption was used to protect the molten bath, as well as the cooling metal of the seam. The welding speed (V_w) varied in the range of 0.8–3.0 m/min. The laser radiation power P varied in the range of 2.0–4.0 kW.

3. RESULTS AND DISCUSSION

The structure of the CR1000Y1370T-CH-EG53/53-U steel in the state after rolling, thermomechanical treatment and application of zinc coating in the direction along and across the rolling direction, as well as selected samples after various modes and methods of welding, was investigated.

After laser welding, four best samples were selected according to visual inspection, which were welded according to these modes: 1482.1, 1481.2, 1481.4, 1481.6 (of which 1482.1 is along the roll, others are across). The general appearance of samples made by laser welding, after selection and cutting, is shown in Fig. 5, *a*. Samples 1, 5, 8 (Fig. 5, *b*) and 3, 6, 9 (Fig. 5, *c*) were selected for research after contact-spot and argon-arc spot welding respectively. Even at the stage sample production, some joints, made by the argon-arc spot welding method were partially destroyed (Fig. 5, *c*), indicating an incorrectly selected welding mode.

TABLE 3. Argon-arc welding modes and their results.

Sample	Welding mode	Results
1	2	3
1	Tungsten electrode diameter $\varnothing_{ele} = 2.4$ mm, sharpening angle 30°, argon consumption rate $Q = 12$ l/min, welding time $t_w = 1.8$ s, current rise time $t_{cr} = 0.1$ s, current fall time $t_{cf} = 0.2$ s, welding current $I_w = 55$ A, arc voltage $U = 12$ V	Incomplete formation of the spot core. More powerful welding mode required
2	Tungsten electrode diameter $\varnothing_{ele} = 2.4$ mm, sharpening angle 30°, argon consumption rate $Q = 12$ l/min, welding time $t_w = 1.8$ s, current rise time $t_{cr} = 0.1$ s, current fall time $t_{cf} = 0.2$ s, welding current $I_w = 65$ A, arc voltage $U = 13$ V	Incomplete formation of the spot core. More powerful welding mode required
3	Tungsten electrode diameter $\varnothing_{ele} = 2.4$ mm, sharpening angle 30°, argon consumption rate $Q = 12$ l/min, welding time $t_w = 2.0$ s, current rise time $t_{cr} = 0.1$ s, current fall time $t_{cf} = 0.2$ s, welding current $I_w = 75$ A, arc voltage $U = 12$ V	Spot weld formed
4	Tungsten electrode diameter $\varnothing_{ele} = 2.4$ mm, sharpening angle 30°, argon consumption rate Q =12 l/min, welding time $t_w = 2.2$ s, current rise time $t_{cr} = 0.1$ s, current fall time $t_{cf} = 0.2$ s, welding current $I_w = 80$ A, arc voltage $U = 12.5$ V	Spot weld formed.
5	Tungsten electrode diameter $\varnothing_{ele} = 2.4$ mm, sharpening angle 30°, argon consumption rate $Q = 12$ l/min, welding time $t_w = 2.4$ s, current rise time $t_{cr} = 0.1$ s, current fall time $t_{cf} = 0.2$ s, welding current $I_w = 80$ A, arc voltage $U = 12.5$ V	Spot weld formed
6	Tungsten electrode diameter $\varnothing_{ele} = 2.4$ mm, sharpening angle 30°, argon consumption rate $Q = 12$ l/min, welding time $t_w = 2.4$ s, current rise time $t_{cr} = 0.1$ s, current fall time $t_{cf} = 0.2$ s, welding current $I_w = 85$ A, arc voltage $U = 12$ V	Spot weld formed.

Continuation of Table 3.

1	2	3
7	Tungsten electrode diameter $\varnothing_{ele} = 2.4$ mm, sharpening angle 30°, argon consumption rate $Q = 12$ l/min, welding time $t_w = 2.4$ s, current rise time $t_{cr} = 0.1$ s, current fall time $t_{cf} = 0.2$ s, welding current $I_w = 95$ A; arc voltage $U = 13$ V	Upper plate welded through. Welding mode is excessive
8	Tungsten electrode diameter $\varnothing_{ele} = 2.4$ mm, sharpening angle 30°, argon consumption rate $Q = 12$ l/min, welding time $t_w = 2.4$ s, current rise time $t_{cr} = 0.1$ s, current fall time $t_{cf} = 0.2$ s, welding current $I_w = 90$ A, arc voltage $U = 13.5$ V	Upper plate welded through. Welding mode is excessive
9	Tungsten electrode diameter $\varnothing_{ele} = 2.4$ mm, sharpening angle 30°, argon consumption rate $Q = 12$ l/min, welding time $t_w = 2.5$ s, current rise time $t_{cr} = 0.1$ s, current fall time $t_{cf} = 0.2$ s, welding current $I_w = 80$ A, arc voltage $U = 13$ V	Spot weld formed

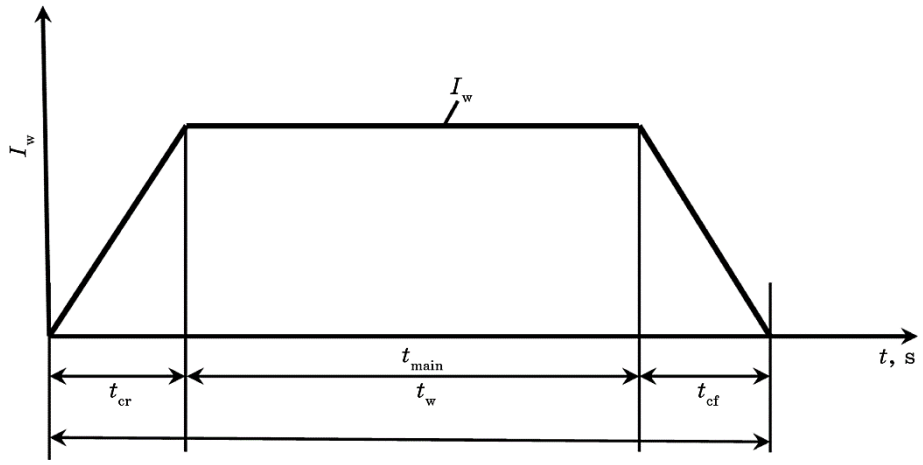

Fig. 4. Argon-arc welding cyclogram.

3.1. Metallographic Study of AHSS Steels after Laser Welding

Macroscopic studies of the welded joint performed according to 1481.1 mode showed a high-quality connection of metal sheets without delaminations, defects, nor the formation of cracks and pores.

Metallographic studies of the metal of the welded joint of CR1000Y1370T-CH-EG53/53-U steel after laser welding according to the 1482.1 mode showed that the structure of the weld metal is ferrite-bainite. In the seam zone, the grain size differs from the base metal. The

TABLE 4. Laser-welding modes for experimental samples.

Sample number	Joint type, sample preparation	Welding mode	Result
1481.1	Overlap joint $h = 1.2$ mm	$V_w = 3$ m/min (50.0 mm/s), $P = 4$ kW	Complete fusion
1481.2	Overlap joint $h = 1.2$ mm	$V_w = 1.5$ m/min (25.0 mm/s), $P = 2$ kW	Incomplete fusion
1481.3	Overlap joint $h = 1.2$ mm	$V_w = 0.8$ m/min (13.33 mm/s), $P = 2$ kW	Complete fusion
1481.4	Overlap joint $h = 1.2$ mm, sample cleaned of coating	$V_w = 0.8$ m/min (13.33 mm/s), $P = 2$ kW	Complete fusion
1481.5	Overlap joint $h = 1.2$ mm, sample cleaned of coating	$V_w = 3$ m/min (50.0 mm/s), $P = 4$ kW	Incomplete fusion
1481.6	Overlap joint $h = 1.2$ mm	$V_w = 1.9$ m/min (31.67 mm/s), $P = 3$ kW	Complete fusion
1481.7	Overlap joint $h = 1.2$ mm, sample cleaned of coating	$V_w = 1.9$ m/min (31.67 mm/s), $P = 3$ kW	Complete fusion

size of the grains in the seam is 30–40 μm, and the structure of the seam is blocky with the orientation of the crystallites along the direction of heat removal, but with a grain shape close to equiaxed (Fig. 6).

According to the results of durometric studies (Vickers method, 50 g load), it was established that the hardness of the base metal is 3707 ± 225 MPa. Studies of the hardness of the characteristic zones of the welded joint showed that the hardness of the seam was 3298 ± 130 MPa, while the coarse grain areas had a lower hardness (2548 ± 130 MPa) than the areas of fine grain (3413 ± 140 MPa). The difference in hardness values is explained by the fact that smaller grains have a bainite structure, which is characterized by the higher level of hardness, while, in the coarse grain areas, a larger amount of ferrite phase exists, which imitates the primary austenite grains. A more dispersed grain size with more bainite is a result of a higher cooling rate.

The use of scanning electron microscopy made it possible to determine the features of the ferrite–bainite structure, which is formed in various sections of the welded joint of AHSS steel during laser welding (Fig. 7).

It was established that the number of non-metallic inclusions formed in the weld seam zone is greater than that in the main metal.

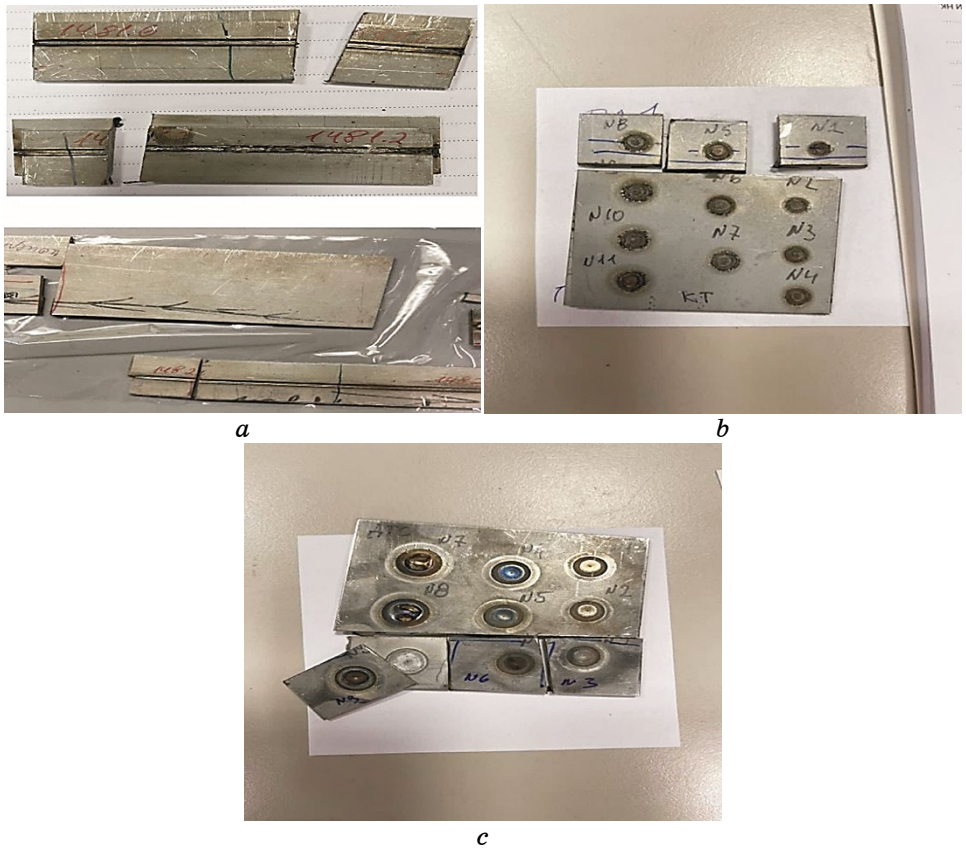

Fig. 5. Appearance of samples after: laser welding (*a*), contact spot welding (*b*), argon-arc spot welding (*c*).

Non-metallic inclusions have a globular shape and are mainly located along the boundaries of bainite packets. Their size is up to 2 μm, which is slightly larger than in the original metal, and may be the result of their agglomeration under the influence of a highly intense heat source during laser welding. The grain size in the seam is of 30–40 μm; in the HAZ of the metal, it is of 10–20 μm.

The study of the welded joint made according to 1481.2 mode showed that due to the formation of a number of iron carbides in the weld metal and the presence of a 'white strip', as evidenced by the results of micro-x-ray spectral analysis (Fig. 8, *a*), the weld is of poor quality. This 'white strip' was formed as a result of an improperly selected welding mode, which did not ensure the evaporation of zinc (which was previously applied as a protective coating) from the surface of the sheet. The results of the x-ray microspectral analysis showed that the zinc content in it is that of around 77–80%.

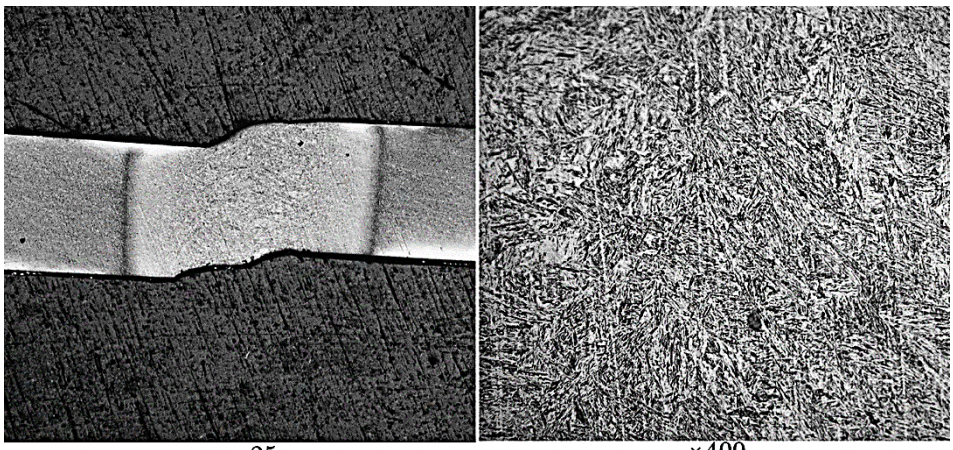

Fig. 6. Macro- (*a*) and microstructure (*b*) (optical microscopy) of the welded joint of AHSS steel according to 1481.1 mode: without etching (*a*), after etching (*b*).

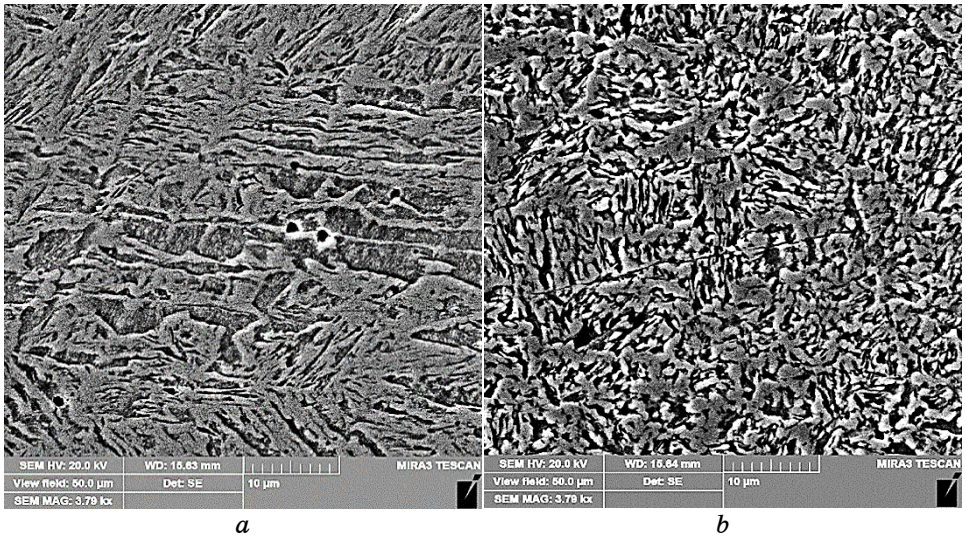

Fig. 7. Microstructure of the welded joint of AHSS steel according to 1481.1 mode: weld metal (*a*), heat-affected zone (electron microscopy) (*b*).

Metallographic studies of the metal of the welded joint made according to 1481.2 mode showed that the structure of the weld metal is ferrite–bainite one (Fig. 8, *b*).

According to the results of durometric studies, it was established that the hardness of the base metal is 3278 ± 160 MPa. Studies of the

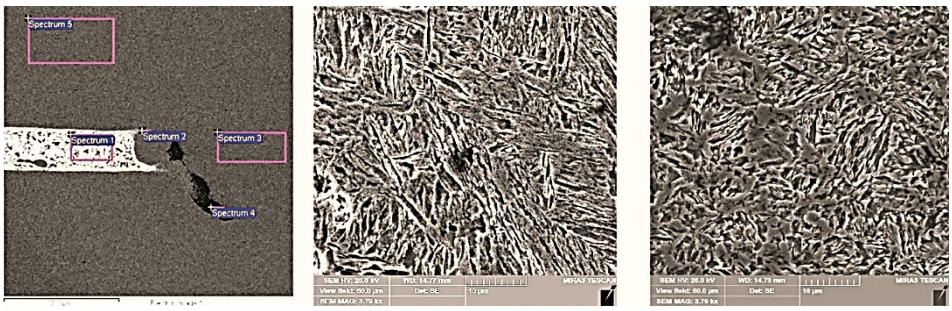

a *b* *c*

Fig. 8. The structure of the welded joint after laser welding according to mode 1481.2: macrostructure (BEI mode) ×100 (*a*), seam metal (*b*), heat-affected zone, ×3000 (*c*).

hardness of the characteristic zones of the welded joint showed that the hardness of the seam was 3849 ± 130 MPa, while the areas of coarse grain had a lower hardness 2960 ± 135 MPa, the areas of fine grain was 3670 ± 107 MPa. The difference in hardness values is attributed to the fact that a smaller grain has a bainite structure, which is characterized by higher hardness, while, in the areas of coarse grain, there is a larger amount of ferrite phase, which imitates the primary austenite grains. The size of the grains is 35–40 μm, which is 10–15% larger than in the previous sample, the size of the grains in the HAZ is 15–25 μm. The size of bainite packets is up to 3 μm.

The study of the welded joint performed according to the 1481.4 mode showed a high-quality fusion of metal sheets without delamination's, defects, or the formation of cracks and pores. After laser welding of the samples according to the 1481.4 mode, a significant number of dispersed regular globular non-metallic inclusions up to 2 μm in size were found in the weld metal. Metallographic studies of the welded joint metal showed that the weld metal structure in this case is also ferrite-bainite (Fig. 9). The size of the grains in the seam is 20–40 μ, the structure of the seam is characteristically blocky with crystallites directed along the direction of heat dissipation, but close to the equiaxed shape.

According to the results of durometric studies, it was established that the hardness of the base metal is 3445 ± 160 MPa. Studies of the hardness of the characteristic zones of the welded joint showed that the hardness of the seam is lower than the previous samples and is 3046 ± 75 MPa, in coarse grain areas the hardness is 2493 ± 55 MPa, in fine grain areas is 3900 ± 270 MPa. Studies have shown that a more dispersed microstructure is formed in the HAZ compared to than in the seam (Fig. 10, *b*, *c*). The grain size is of 20–30 μm.

The study of the welded joint made according to 1481.6 mode showed a combination of metal sheets without delamination, defects,

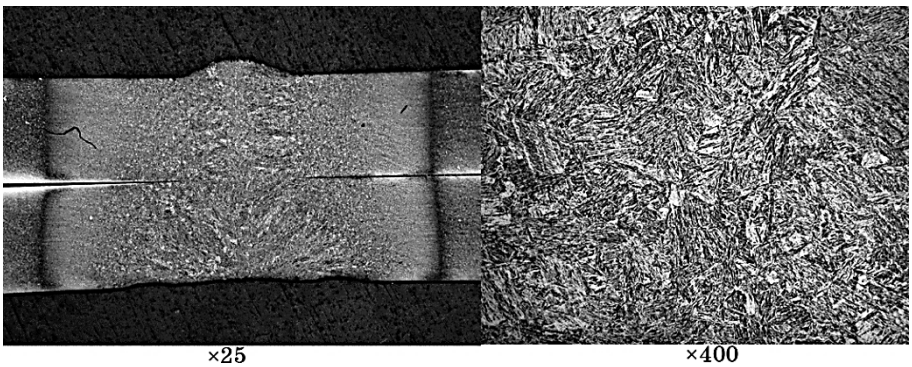

Fig. 9. Macro- (*a*) and microstructure (*b*) (optical microscopy) of the AHSS steel welded joint according to 1482.4 mode.

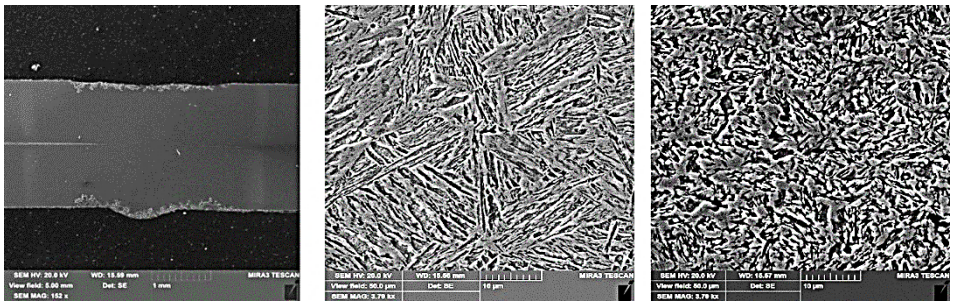

Fig. 10. The structure of the welded joint after laser welding according to mode 1481.4: macrostructure ×100 (*a*), metal structure of the seam (*b*), HAZ metal, ×3000 (*c*).

the formation of cracks and pores, but similarly to the sample that was welded according to mode 1481.2 (Fig. 8), a clear white line was found in the metal of the welded joint, which, according to the results of spectral analysis, indicates a high (70–75%) zinc content in it. As in the previous case, this is the result of incomplete removal of zinc from the surface of the sheet, the coating of which was previously applied for corrosive protection.

Metallographic studies of the metal of the welded joint (Fig. 11) made according to 1481.6 mode show that the weld-metal structure, like in previous samples, is a ferrite–bainite block with a characteristic growth of crystallites along the direction of heat dissipation, but the parameters in this case did not ensure the formation of a high-quality joint.

According to the results of durometric studies, it was established that the hardness of the base metal is 3097 ± 165 MPa, the hardness of

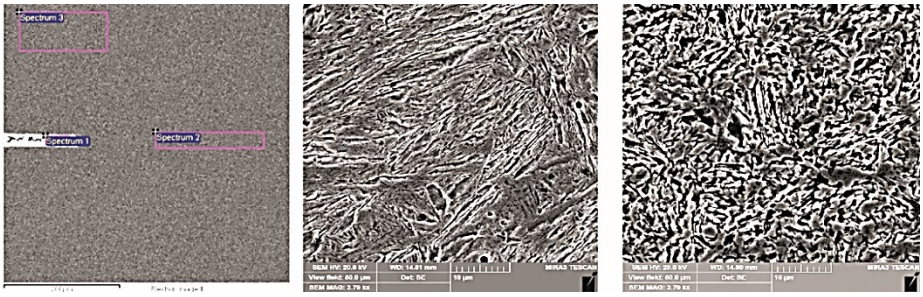

a *b* *c*

Fig. 11. The structure of the welded joint after laser welding according to mode 1481.6: macrostructure (BEI mode) ×100 (*a*), seam metal (*b*), heat-affected zone, ×3000 (*c*).

the seam is 3016 ± 150 MPa, in the areas with coarse grain is 2770 ± 170 MPa, in areas with fine grain is 3342 ± 165 MPa. The study of the microstructure showed the formation of a dispersed structure, the size of the grains is 20–30 μm (Fig. 11, *b*); however, as a result of the thermal effect and increased cooling rate in the 1481.6 mode, the equiaxial structure did not form.

3.2. Metallographic Studies of AHSS Steel after Argon-Arc Spot Welding

According to the selected regimes, 5 out of 9 joints were successfully formed, in two the core of the spot was not completely formed, and in the other two—the top plate was burned through, which indicates an excessively powerful welding mode. In order to avoid the formation of a hole in the upper welded sheet, it is necessary to create technological devices that will allow the sheets to be pressed together without an air gap. Poor-quality pressing of welded parts leads to the appearance of such defects, even when proper welding modes are used.

Further metallographic studies showed the formation of hardening structures in the weld metal of this steel, which is associated with the fact that welding was performed on harsh (for the metal) modes. To avoid this, utilization of pulse mode welding is necessary, allowing us to control the thermal cycle of welding. In this case, welding should be carried out with a lower heat input, which would allow us to obtain welded joints with the specified parameters and the structure of the weld metal without creation of martensite. The following welding of this steel must be carried out on softer welding modes, which prevent the appearance of hardening structures in the weld metal. That is, *via* control the cooling rate of the welded joint during welding.

It was also established that during argon-arc spot welding it is not

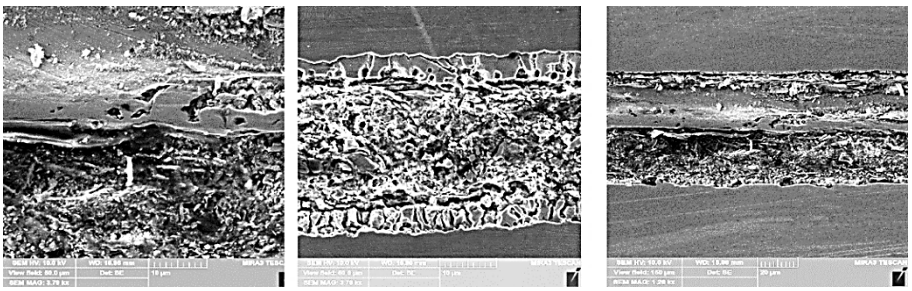

a *b* *c*

Fig. 12. The structure of the welded joint after argon-arc spot welding by modes: joint 1 (*a*), joint 5 (*b*), joint 8. ×100 (*c*).

possible to avoid burning of the zinc coating on the outer surface of the sample. This is the case because it evaporates under the action of the welding arc. Another disadvantage of argon-arc spot welding is the presence of a crater in the middle of the welded spot joint.

Unfortunately, after argon-arc spot welding in all modes, even in the samples, which, according to visual inspection, have looked promising, according to results of metallographic studies, the welding fusion did not occur.

Layering, formation between the surfaces of agglomeration sheets (with an apparent high zinc content), cracks, *etc.* were detected (Fig. 12). Further studies of the quality of the structure, including durometric ones, were not conducted due to their impracticality. It was concluded that the proposed welding modes need significant correction.

3.3. Metallographic Studies of AHSS Steel after Contact Spot Welding

The selected welding modes allowed for a formation of a high-quality joint with a given spot diameter size of 5–6 mm, however, contact spot welding was performed using welding modes, sufficiently harsh for the metal, leading to the appearance of hardening structures in the welded joint metal, as well as the burning of the zinc coating on the outer surfaces of the samples, as shown by further microstructural studies. In order to obtain spot welds with a minimum content of hardening structures, it is necessary to perform welding in softer modes, as well as to apply a pulsed welding current. Conducting welding in such modes will minimize the burnout of the tin coating on the outer sides of the plates.

Macroscopic studies of the welded joint performed according to mode No. 1 by contact spot welding established the connection of metal sheets without delamination, defects, the formation of cracks and pores, however, more thorough studies of the metal structure using SEM revealed unevenness and delamination of the structure in the weld metal. X-ray

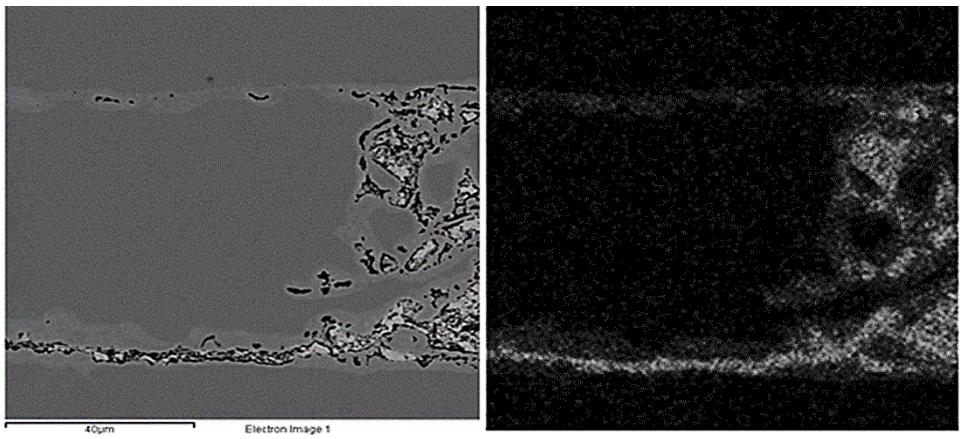

a *b*

Fig. 13. The nature of zinc distribution in the welded joint produced by contact spot welding (mode No. 1): seam microstructure (*a*), zinc distribution map, ×500 (*b*).

spectral analysis revealed zinc residues in the joint area (Fig. 13).

Unlike all previous samples obtained by contact spot welding, the revealed structure of the weld metal is bainite–martensitic one. This indicates that the welding mode was sufficiently intense, during which rapid heating and cooling has occurred. According to the results of durometric studies, the formation of bainite-martensitic and even areas of martensitic structure was confirmed. Thus, it was established that the hardness of the seam is 5402 ± 220 MPa, in the coarse grain areas the hardness is 4899 ± 270 MPa, in the areas with fine grain is 5338 ± 90 MPa, which is significantly different from the hardness of the original metal.

The study of the microstructure of the sample performed by contact-spot welding according to mode No. 1 showed the formation of bainite–martensitic and fine-martensitic (thin-plate) structures in the metal of the welded joint (Fig. 14). The size of the grains (bainite packets) is 5–10 µm, and the length of the needles is 2–5 µm, which confirms its formation at a high rate of heating and cooling. Obviously, it is necessary to select a more 'soft' welding mode, which, however, would ensure the removal of the zinc coating.

The study of the welded joint performed according to contact spot welding mode No. 5 established the connection of metal sheets without delamination, defects, the formation of cracks and pores, however, similar to the aforementioned mode No. 1, unevenness and delamination were found in the structure of the weld metal. X-ray spectral analysis revealed a clear area with increased zinc content along the entire length of the joint zone.

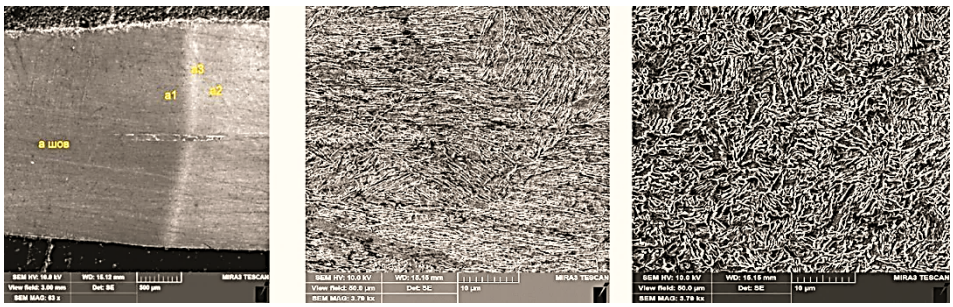

a *b* *c*

Fig. 14. The structure of the welded joint after contact spot welding according to No. 1 welding mode: macrostructure (BEI mode) ×100 (*a*), seam metal (*b*), heat-affected zone metal, ×3000 (*c*).

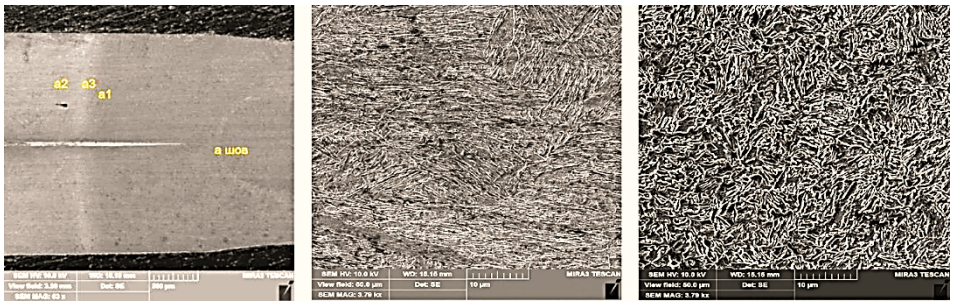

a *b* *c*

Fig. 15. The structure of the welded joint after contact spot welding according to mode No. 5: macrostructure (BEI mode) ×100 (*a*), seam metal (*b*), heat-affected zone metal, ×3000 (*c*).

Metallographic studies of the metal of the welded joint using the contact spot welding mode No. 5 mode showed that the structure of the weld metal is bainite-martensitic. According to the results of durometric studies, the formation of the bainite-martensitic and even martensitic structure was confirmed. Thus, the hardness of the seam is 5250 ± 225 MPa, in coarse grain areas, the hardness is 5177 ± 65 MPa, in fine grain areas, and it is 5267 ± 187 MPa, which is significantly different from the hardness of the original metal.

Microstructure studies showed the formation of bainite-martensitic and martensitic (thin-plate) structures in the metal of the welded joint (Fig. 15). The size of grains (bainite packets) is 7–12 μm, and the length of martensite plates is up to 5 μm.

Metallographic studies of the metal of the welded joint made according to contact spot welding mode number 8 showed that the structure of the weld metal is bainite-martensitic. Similarly to the previous re-

sults of the analysis of welded joints of contact-spot welding, the results of durometric studies confirmed the formation of a bainitic-martensitic and even martensitic structure, but with a slightly lower level of hardness. As such, the hardness of the weld is 4760 ± 300 MPa, coarse grain is 3664 ± 140 MPa, fine grain is 4944 ± 260 MPa, which may indicate a 'softer' welding mode, however, it is not optimal for the formation of a uniform quality structure in this type of steel.

Microstructure studies confirmed the formation of a dispersed bainite-martensitic and martensitic (needle) structure in the metal of the welded joint (Fig. 16). The size of the grains (bainite packets) is up to 10 μm, and the length of the martensitic formations is up to 5 μm.

Conducted research on a series of welding of 1.2 mm thick sheet CR1000Y1370T-CH-EG53/53-U steel (wt.: 0.23% C, 2% Si, 3% Mn, 0.015–2% Al, 1% Cr + Mo, 0.15% Ti + Nb, 0.2% Cu) (manufactured by Voelstalpine (Austria)) showed the fundamental possibility of applying modern methods of joining steels by laser, contact-spot and argon-arc spot welding.

Metallographic studies showed that the best-welded joints were obtained using laser welding in modes 1482.1 and 1481.4 (along and across the rolling direction). According to the selected modes, it was possible to ensure the formation of a dispersed structure with an acceptable level of hardness of up to 4000 MPa, while avoiding the formation of critical martensitic structures. In addition, it was possible to ensure the evaporation of zinc from the coating of the sheet along the entire length of the welded joint, in contrast to modes 1481.2 and 1481.6.

Application of contact-spot and argon-arc spot welding did not show the expected result. During argon-arc spot welding, complete weld fusion metal sheets could not be achieved. During contact spot welding, critical structures of martensite with a high (up to 5400 MPa) level of hardness, as well as formations of zinc inclusions and strips in the seam

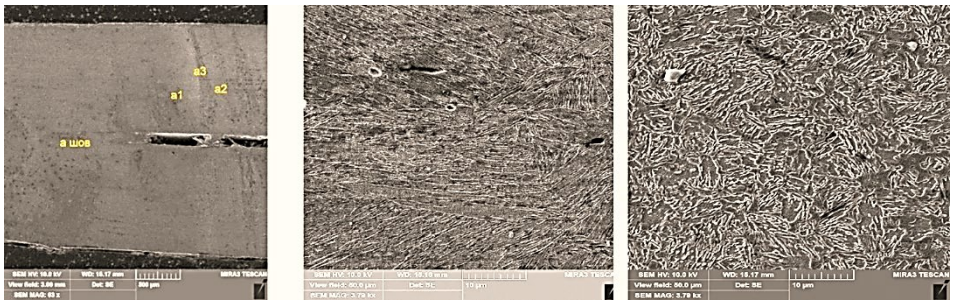

a *b* *c*

Fig. 16. The structure of the welded joint after contact spot welding according to mode No. 8: macrostructure (BEI mode) ×100 (*a*), seam metal (*b*), heat-affected zone metal, ×3000 (*c*).

zone were found and considered unacceptable. The formation of agglomerates and unevenness of the structure were observed. In conclusion, the chosen modes of these welding technologies require further refinement.

4. CONCLUSION

Conducted research on a series of welding of 1.2 mm thick sheet metal out of CR1000Y1370T-CH-EG53/53-U steel (wt.: 0.23% C, 2% Si, 3% Mn, 0.015–2% Al, 1% Cr + Mo, 0.15% Ti + Nb, 0.2% Cu) (manufactured by Voelstalpine, Austria) showed the fundamental possibility of applying modern methods of joining steels by laser, contact-spot and argon-arc spot welding.

High-quality welded joints were obtained using laser welding with the formation of a dispersed ferrite–bainite structure with an acceptable (up to 4000 MPa) level of hardness without formation of martensitic-type structures and zinc evaporation from the sheet coating along the entire length of the welded joint. When using contact-spot and argon-arc spot welding according to the selected modes, it was not possible to obtain high-quality welded joints due to delamination and zinc coating residues, so the selected modes of these types of welding turned out to be ineffective deemed to require further refinement.

REFERENCES

1. J. Galán, L. Samek, P. Verleysen, K. Verbeken, and Y. Houbaert, *Revista De Metalurgia*, **48**, No. 2: 118 (2012).
2. G. Park, S. Jeong, and C. Lee, *Metals Mater. Int.*, **27**: 2046 (2021).
3. F. Bayock, P. Kah, A. Salminen, M. Belinga, and X. Yang, *Rev. Adv. Mater. Sci.*, **59**, No. 1: 54 (2020).
4. F. Bayock, P. Kah, B. Mvola, and P. Layus, *Rev. Adv. Mater. Sci.*, **58**, No. 1: 38 (2019).
5. J. Hall and J. Fekete, *Automotive Steels* (Eds. Radhakanta Rana and Shiv Brat Singh) (Elsevier: 2017), p. 19.
6. T. Hilditch, S. Toman, and D. Fabijanic, *Materials Forum*, **31**: 24 (2007).
7. M. Singh, *Int. J. Emerging Technol. Adv. Eng.*, **6**, No. 7: 246 (2016).
8. D. Michell, A. Centeno, and H. Goldenstein, *Mater. Sci. Forum*, **941**: 413 (2018).
9. M. N. M. Salleh, M. Ishak, and M. M. Quazi, *Technological Advancement in Mechanical and Automotive Engineering* (Eds. M. Y. Ismail, M. S. M. Sani, S. Kumarasamy, M. A. Hamidi, and M. S. Shaari) (Singapore: Springer: 2023), p. 279.
10. S. Cecchel, *SAE Int. J. Mater. Manufact.*, **14**, No. 1: 81 (2021).
11. M. Shome and M. Tumuluru, *Welding and Joining of Advanced High Strength Steels (AHSS)* (Eds. M. Shome and M. Tumuluru) (Elsevier: 2015), p. 204.
12. D.-Y. Choi and Y.-G. Kim, *J. KWJS*, **27**, No. 2: 125 (2009).
13. M. I. Khan, *Spot Welding of Advanced High Strength Steels* (Waterloo: 2007).
14. M. Tümer, C. Schneider-Brökamp, and N. Enzinger, *J. Manufact. Processes*, **82**:

203 (2022).
15. A. Guzanová, D. Draganovská, M. Tomáš, E. Janoško, and R. Moro, *Acta Mechanica Slovaca*, **24**, No. 4: 24 (2020).
16. Y. S. Kim, Y. S. Kim, K. C. Park, J. B. Nam, T. J. Kim, and B. H. Lee, *J. Korean Society for Technology of Plastics*, **26**, No. 4: 246 (2017).
17. A. Bernatskyi and V. Khaskin, *History of Science and Technology*, **11**, No. 1: 125 (2021).
18. A. Bernatskyi, O. M. Berdnikova, V. Sydorets, V. Kostin, and O. Kushnarova, *Solid State Phenomena*, **313**: 106 (2021).
19. V. Khaskin, A. Bernatskyi, O. Siora, and O. Nikulin, *Metallofiz. Noveishie Tekhnol.*, **33**: 561 (2011).
20. X. Hu and Z. Feng, *Advanced High-Strength Steels-Basic and Application in the Automotive Industry* (Oak Ridge: Oak Ridge National Laboratory: 2021).
21. K. A. Manoharan, M. M. Quazi, M. N. Bashir, M. N. M. Salleh, A. Q. Zafiuddin, and R. Linggamm, *Int. J. Technol. Eng. Studies*, **6**, No. 1: 23 (2020).
22. D. Lesyk, S. Martinez, B. Mordyuk, V. Dzhemelinskyi, and O. Danyleiko, *Advances in Design, Simulation and Manufacturing II* (Eds. V. Ivanov, J. Trojanowska, J. Machado, O. Liaposhchenko, J. Zajac, I. Pavlenko, M. Edl, and D. Perakovic) (Springer: 2019), p. 188.
23. V. Pozniakov, L. Markashova, O. Berdnikova, T. Alekseienko, and S. Zhdanov, *Materials Science Forum*, **927**: 29 (2018).
24. D. Kritskiy, O. Pohudina, M. Kovalevskyi, Ye. Tsegelnyk, and V. Kombarov, *Integrated Computer Technologies in Mechanical Engineering — 2021* (Eds. M. Nechyporuk, V. Pavlikov, and D. Kritskiy) (Springer: 2021), p. 924.
25. A. Bernatskyi, V. Sydorets, O. Berdnikova, I. Krivtsun, and O. Kushnarova, *Solid State Phenomena*, **313**: 94 (2021).
26. O. Strelko, O. Solovyova, Yu. Berdnychenko, H. Kyrychenko, and L. Solovyova, *Acta Scientiarum Polonorum Administratio Locorum*, **22**, No. 2: 263 (2023).
27. I. Bondarenko, A. Severino, I. Olayode, T. Campisi, and L. Neduzha, *Infrastructures*, **7**, No. 9: 124 (2022).
28. H. Kyrychenko, O. Strelko, and Yu. Berdnychenko, *IOP Conf. Series: Earth and Environmental Sci.*, **666**, No. 4: 042054 (2021).
29. O. Fomin, A. Lovska, and A. Horban, *History of Science and Technology*, **11**, No. 2: 351 (2021).
30. O. Fesovets, O. Strelko, Yu. Berdnychenko, S. Isaienko, and O. Pylypchuk, *Proc. 23rd Int. Sci. Conf. 'Transport Means 2019' (October 02–04, 2019)* (Palanga: 2019), part 1, p. 381.
31. A. Bernatskyi, O. Siora, M. Sokolovskyi, V. Lukashenko, T. Nabok, N. Shamsutdinova, and V. Bondarieva, *Proc. 26th Int. Sci. Conf. 'Transport Means 2022' (5–7 October, 2022)* (Palanga: 2022), part 1, p. 89.
32. O. Aksonov, Ye. Tsegelnyk, V. Kombarov, S. Plankovskyy, and Y. Aksonov, *Proc. Int. Conf. 'Smart Technologies in Urban Engineering–STUE-2022' (June 9–11, 2022)* (Kharkiv: 2022), p. 547.
33. P. Gontarovskyi, N. Smetankina, N. Garmash, and I. Melezhyk, *Integrated Computer Technologies in Mechanical Engineering — 2020* (Eds. P. Gontarovskyi, N. Smetankina, N. Garmash, and I. Melezhyk) (Springer: 2020), p. 609.
34. Y. Milman, B. Mordyuk, K. Grinkevych, S. Chugunova, I. Goncharova, A. Lukyanov, and D. Lesyk, *Progress in Physics of Metals*, **21**: 554 (2020).